JOURNAL OF COMPUTATIONAL PHYSICS 105, 72–82 (1993)

Dispersion and Group Velocity in Numerical Schemes for Three-Dimensional Hydrodynamic Equations

YUHE SONG* AND TAO TANG

Department of Mathematics and Statistics, Simon Fraser University, Burnaby, British Columbia, Canada V5A 1S6

Received May 21, 1991; revised May 12, 1992

We investigate dispersion and group velocity relations of numerical schemes for the three-dimensional hydrodynamic equations by using the transform function method. The numerical methods are developed for two of Arakawa's spatial grid types, namely B grid and C grid, using a spectral method in the vertical direction. One of our results is that if the horizontal scale length is greater than the Rossby radius of deformation then the B grid is more appropriate than the commonly used C grid.

1. INTRODUCTION

Within the area of oceanographic flows, the early numerical models were for the two-dimensional hydrodynamic equations in which the current structure was removed by integrating through the vertical from the sea surface to the sea bed, obtaining what are called the shallow water equations. These models were primarily used to study changes in an elevation due to tides and meteorological events (storm surge models). A variety of computational methods have been developed to obtain numerical solutions of these equations (see, e.g., [1, 2, 8]).

In recent years there has been considerable interest in developing full three-dimensional flow models, since more detailed information on the current is required in practice (see, e.g., [10, 11, 14–16]). For example, the surface velocity determines the motion of an oil slick and for a wind-driven flow, for instance, the surface velocity differs very much from the depth-averaged flow.

In solving the hydrodynamic model equations numerically, the numerical errors not only come from the truncation error but also from the numerical dispersion. In order to obtain accurate numerical solutions, we need to construct high order schemes with low numerical dispersion (see, e.g., [20, 25, 26]). The main purpose of this work is to investigate the behaviors of the numerical dispersion and group velocity for some widely used hybrid schemes in solving three-dimensional hydrodynamic equations.

In general, there are five numerical grids, usually refered to as A–E grids, which are obtained by appropriate arrangements of the dependent variables in the horizontal directions (see, e.g., [1, 2] and Fig. 1). In the one-dimensional case, Winninghoff [29] and Schoenstadt [23] carried out extensive investigations of geostrophic adjustment for these five schemes. Their analysis suggests that the B grid is the most satisfactory one for one-dimensional models.

Arakawa and Lamb [1] studied the applications of the A–E grids for two-dimensional models. They found that, in contrast to the one-dimensional case, the C grid is the best one among the five schemes when they are employed in the two-dimensional calculations. Since then the C grid (sometimes called the Arakawa C grid) has been used extensively in practical calculations, starting with the two-dimensional algorithms [6, 9, 19] down to the more recent three-dimensional algorithms [3, 13, 15, 16] and including the algorithms based on the spectral method in the vertical direction [4, 5, 10, 11, 12]. However, Jamart and Ozer [12] found that the C grid might lead to spurious numerical boundary layers if the spectral method is used in the vertical direction unless the Coriolis terms are treated specially on the boundaries. Since the two horizontal velocity components are computed at different spatial points with a C grid, it is necessary to average the Coriolis term in each momentum equation over the four neighboring points at which the opposite velocity component is computed. Adjacent to a coast, one or more of these four points will actually lie on the coast, and the velocity components at such points are maintained at zero by the usual algorithms. The result is that the four-point average gives an incorrect value for the interior point, and this leads to spurious velocities near the coast. In order to handle this problem Song [24] compared the A–E grids by solving a model problem for which the exact solution can be found analytically. The numerical

* Current address: Institute of Marine & Coastal Sciences, Rutgers University, New Brunswick, NJ08903-0231, USA.

0021-9991/93 $5.00

results suggest that the B grid provides a viable alternative to the C grid, with significant advantages when the spectral method is employed.

To have a better understanding of the B and C grids in three-dimensional calculations, a general analysis is required under certain theoretical frameworks. The transfer function approach introduced by Schoenstadt [22] has been used to study the behavior of the semi-discrete shallow water equations which are solved by the finite-difference method [22, 23], the finite-element method [28], and the Turkel–Zwas scheme [21]. As a useful tool in analyzing numerical schemes, the transfer function approach leads to important insights into the behavior of the discretization scheme in terms of comparison between continuous and discrete amplitude, phase, and group velocity coefficients. In this work we shall apply the transfer function approach to a mixed finite-difference spectral method for the numerical solutions of the three-dimensional hydrodynamic equations. In Section 2 of this paper, we introduce the mathematical equations which are to be solved numerically. In Section 3 the numerical discretization is presented. In Section 4 the numerical schemes are transformed into the phase space and the dispersion relations are solved. Finally, in Section 5 the numerical results of the transfer function analysis for the numerical schemes are compared to those of the transfer function analysis for the differential model.

2. BASIC EQUATIONS

We use xyz as Cartesian coordinates with the z-axis pointing vertically upwards and the xy-plane occupying the undisturbed water surface. The horizontal momentum equations and the integrated equation of continuity for a homogeneous sea, including the nonlinear terms but neglecting shear in the horizontal direction and the direct influence of tide generating forces, may be written as

$$\frac{\partial u}{\partial t}+u\frac{\partial u}{\partial x}+v\frac{\partial u}{\partial y}+w\frac{\partial u}{\partial z}-fv = -g\frac{\partial \zeta}{\partial x}+\frac{\partial}{\partial z}\left(N\frac{\partial u}{\partial z}\right), \tag{2.1}$$

$$\frac{\partial v}{\partial t}+u\frac{\partial v}{\partial x}+v\frac{\partial v}{\partial y}+w\frac{\partial v}{\partial z}+fu = -g\frac{\partial \zeta}{\partial y}+\frac{\partial}{\partial z}\left(N\frac{\partial v}{\partial z}\right), \tag{2.2}$$

$$\frac{\partial \zeta}{\partial t}+\frac{\partial}{\partial x}\left(\int_{-h}^{\zeta} u\,dz\right)+\frac{\partial}{\partial y}\left(\int_{-h}^{\zeta} v\,dz\right)=0, \tag{2.3}$$

where $u=u(x, y, z, t)$ and $v=v(x, y, z, t)$ are the horizontal velocity components in x and y directions, respectively, $w=w(x, y, z)$ is the vertical velocity component, $h=h(x, y)$ is the water depth, $\zeta=\zeta(x, y, t)$ is the surface elevation, $N=N(x, y, z, t)$ is the vertical eddy viscosity, f is the Coriolis parameter, and g is the acceleration due to gravity. It is required to solve Eqs. (2.1)–(2.3), subject to the boundary conditions on the sea surface and at the sea bed. The surface conditions, evaluated at $z=\zeta$, are

$$\rho N\frac{\partial u}{\partial z}=\tau_x, \qquad \rho N\frac{\partial v}{\partial z}=\tau_y, \tag{2.4}$$

where ρ is the fluid density and τ_x and τ_y are the components of wind stress acting on the free surface in the x and y directions, respectively. Correspondingly, at the sea bed, $z=-h$, the boundary conditions are

$$\begin{aligned} N\frac{\partial u}{\partial z}&=(\kappa_1+\kappa_2\sqrt{u^2+v^2})u,\\ N\frac{\partial v}{\partial z}&=(\kappa_1+\kappa_2\sqrt{u^2+v^2})v, \end{aligned} \tag{2.5}$$

where κ_1 and κ_2 are the coefficients of the linear and quadratic bottom friction, respectively.

In this work we shall concentrate on the linearized form of Eqs. (2.1)–(2.3). It is convenient to use the so-called sigma coordinate which is defined by $\sigma=(z+h)/H$, where $H=h+\zeta$ is the total water depth. Using this transform and approximating H by h (note that ζ is very small in comparison with H), we obtain the linear counterpart of Eqs. (2.1)–(2.3),

$$\frac{\partial u}{\partial t}-fv+g\frac{\partial \zeta}{\partial x}=h^{-2}\frac{\partial}{\partial \sigma}\left(N\frac{\partial u}{\partial \sigma}\right), \tag{2.6}$$

$$\frac{\partial v}{\partial t}+fu+g\frac{\partial \zeta}{\partial x}=h^{-2}\frac{\partial}{\partial \sigma}\left(N\frac{\partial v}{\partial \sigma}\right), \tag{2.7}$$

$$\frac{\partial \zeta}{\partial t}+\frac{\partial}{\partial x}\left(h\int_0^1 u\,d\sigma\right)+\frac{\partial}{\partial y}\left(h\int_0^1 v\,d\sigma\right)=0. \tag{2.8}$$

The wind stress in (2.4) will be set equal to zero since the linear boundary conditions can be easily transformed to zero (see [17]). The bottom condition (2.5) is usually calculated explicitly in time (e.g, [16, 18]). It can also be simply set equal to zero (e.g., [7]). This simplicity allows using the vertical spectral method to decouple the barotropic component (depth-averaged flow) from the baroclinic components (vertical perturbation flow) and reduces the numerical difficulty. Since the friction coefficients are very small in practice, accurate numerical solutions can still be obtained under this assumption.

If we ignore the wind force on the surface and the bottom friction, then the boundary conditions become

$$\frac{\partial u}{\partial \sigma}=0, \qquad \frac{\partial v}{\partial \sigma}=0, \qquad \sigma=0, \qquad \sigma=1. \tag{2.9}$$

3. HYBRID NUMERICAL SCHEMES

3.1. *Spectral Method in the Vertical Direction*

The fundamental idea of the spectral method for the discretization in the vertical direction is to expand the velocity components in terms of an appropriate set of basis functions. Following [10, 11, 17, 18], we consider the Sturm–Liouville problem

$$\frac{\partial}{\partial \sigma}\left(N\frac{\partial \phi}{\partial \sigma}\right)+\lambda^2\phi=0, \tag{3.1}$$

$$\frac{\partial \phi}{\partial \sigma}=0, \qquad \text{on} \quad \sigma=0, \quad \sigma=1. \tag{3.2}$$

For ease of our theoretical analysis, we assume that the vertical eddy viscosity N depends only on σ throughout of this paper, i.e., $N=N(\sigma)$. Under this assumption, the eigenpairs can be denoted by $\{\lambda_j, \phi_j(\sigma): j=0, 1, \ldots\}$, where the lowest eigenpair is $\lambda_0=0$, $\phi_0=1$. The eigenfunctions are normalized such that

$$\int_0^1 \phi_j(\sigma)^2\, d\sigma=1, \qquad j\geqslant 1.$$

The eigenfunctions then form an orthonormal system, and in particular, orthogonality with ϕ_0 implies that

$$\int_0^1 \phi_j(\sigma)\, d\sigma=0, \qquad j\geqslant 1.$$

We now expand the velocity components in terms of the eigenfunctions:

$$\begin{aligned} u&=\sum_{n=0}^{\infty} a_n(x, y, t)\,\phi_n(\sigma),\\ v&=\sum_{n=0}^{\infty} b_n(x, y, t)\,\phi_n(\sigma). \end{aligned} \tag{3.3}$$

Multiplying Eqs. (2.6) and (2.7) by $\phi_j(\sigma)$ and integrating the resulting equations with the boundary conditions (2.9), we obtain the system for the modal amplitudes,

$$\begin{aligned} &\frac{\partial \zeta}{\partial t}+\frac{\partial}{\partial x}(ha_0)+\frac{\partial}{\partial y}(hb_0)=0,\\ &\frac{\partial a_0}{\partial t}-fb_0+g\frac{\partial \zeta}{\partial x}=0,\\ &\frac{\partial b_0}{\partial t}+fa_0+g\frac{\partial \zeta}{\partial y}=0,\\ &\frac{\partial a_j}{\partial t}+\alpha_j a_j-fb_j=0, \qquad j\geqslant 1,\\ &\frac{\partial b_j}{\partial t}+\alpha_j b_j+fa_j=0, \qquad j\geqslant 1, \end{aligned}$$

where $\alpha_j=(\lambda_j/h)^2$. Further, the transformations $p=ha_0$, $q=hb_0$, $A_j=a_jh\exp(\alpha_j t)$, and $B_j=b_jh\exp(\alpha_j t)$ lead to

$$\frac{\partial \zeta}{\partial t}+\frac{\partial p}{\partial x}+\frac{\partial q}{\partial y}=0, \tag{3.4}$$

$$\frac{\partial p}{\partial t}-fq+gh\frac{\partial \zeta}{\partial x}=0, \tag{3.5}$$

$$\frac{\partial q}{\partial t}+fp+gh\frac{\partial \zeta}{\partial y}=0, \tag{3.6}$$

$$\frac{\partial A_j}{\partial t}-fB_j=0, \qquad j\geqslant 1, \tag{3.7}$$

$$\frac{\partial B_j}{\partial t}+fA_j=0, \qquad j\geqslant 1. \tag{3.8}$$

It should be pointed out that Eqs. (3.4)–(3.6) are the two-dimensional shallow water equations which have been considered by Arakawa and Lamb [1, 2]. In fact, these three equations can be obtained by integrating (2.6)–(2.8) from the sea surface to the sea bed in the vertical direction. They represent the depth-averaged flow while Eqs. (3.7) and (3.8) represent the vertical perturbation flow. In practical calculations, Eqs. (3.4)–(3.8) are coupled with some nonlinear terms, such as the advection terms and the bottom frictions. However, these nonlinear terms are always treated explicitly and for ease of the theoretical analysis they are set equal to zero. Since the three-dimensional flow consists the depth-averaged flow and the vertical perturbation flow, Eqs. (3.4)–(3.8) should be treated as a system of equations in the analysis. Equations (3.4)–(3.8) will be solved subject to the initial conditions

$$p=h\int_0^1 u_0\, d\sigma, \qquad q=h\int_0^1 v_0\, d\sigma, \qquad \zeta=\zeta_0, \qquad t=0,$$

$$A_j=h\int_0^1 u_0\phi_j\, d\sigma, \qquad B_j=h\int_0^1 v_0\phi_j\, d\sigma, \qquad t=0, \quad j\geqslant 1,$$

where u_0 and v_0 are the initial velocity components in the x and y directions, respectively, and ζ_0 is the initial water elevation.

3.2. *Finite Difference Schemes*

In order to obtain semi-discretized schemes for Eqs. (3.4)–(3.8), we need to consider the discretizations in the horizontal direction. Consider the five distributions of the dependent variables h, u, and v, on a square grid illustrated in Fig. 1. As mentioned in Section 1, there are five space grids which are of second order for the correspondingly labeled distribution [1, pp. 181–182]. As discussed in the Introduction we shall concentrate on the analysis for the B and C grids in the present work. The semi-discretized forms for Eqs. (3.4)–(3.8) corresponding to the B grid and the C grid are given as

B grid,

$$\frac{\partial \zeta}{\partial t} + \overline{(\delta_x p)}^y + \overline{(\delta_y q)}^x = 0, \tag{3.9}$$

$$\frac{\partial p}{\partial t} - fq + gh\,\overline{(\delta_x \zeta)}^y = 0, \tag{3.10}$$

$$\frac{\partial q}{\partial t} + fp + gh\,\overline{(\delta_y \zeta)}^x = 0, \tag{3.11}$$

$$\frac{\partial A_j}{\partial t} - fB_j = 0, \qquad j \geq 1, \tag{3.12}$$

$$\frac{\partial B_j}{\partial t} + fA_j = 0, \qquad j \geq 1; \tag{3.13}$$

C grid,

$$\frac{\partial \zeta}{\partial t} + (\delta_x p) + (\delta_y q) = 0, \tag{3.14}$$

$$\frac{\partial p}{\partial t} - f\bar{q}^{xy} + gh(\delta_x \zeta) = 0, \tag{3.15}$$

$$\frac{\partial q}{\partial t} + f\bar{p}^{xy} + gh(\delta_y \zeta) = 0, \tag{3.16}$$

$$\frac{\partial A_j}{\partial t} - f\overline{B_j}^{xy} = 0, \qquad j \geq 1, \tag{3.17}$$

$$\frac{\partial B_j}{\partial t} + f\overline{A_j}^{xy} = 0, \qquad j \geq 1; \tag{3.18}$$

where we define

$$(\delta_x \gamma)_{mn} \equiv (\gamma_{m+1/2,n} - \gamma_{m-1/2,n})/d, \tag{3.19}$$

$$(\bar{\gamma}^x)_{mn} \equiv \tfrac{1}{2}(\gamma_{m+1/2,n} + \gamma_{m-1/2,n}), \tag{3.20}$$

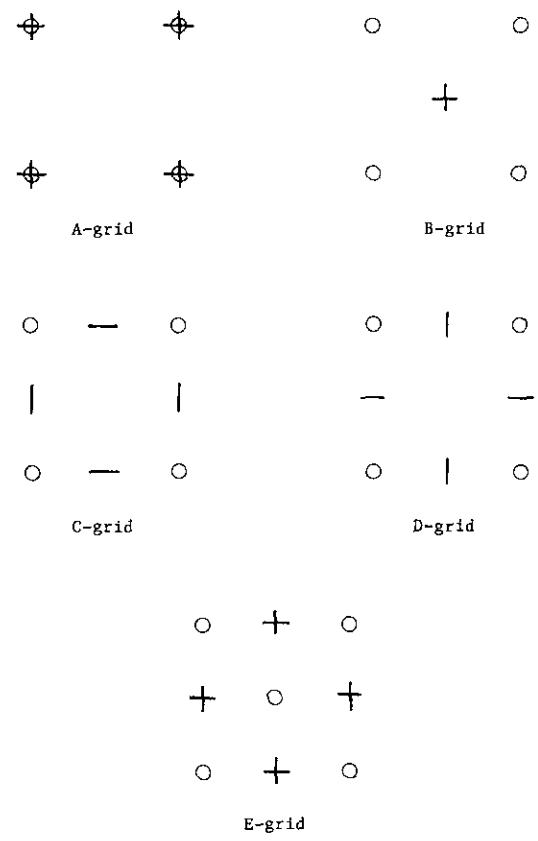

FIG. 1. The five different locations of the horizontal velocity components. ζ-points are indicated by ○, u-points by —, and v-points by |.

and where m and n are the indices of the grid points in the x and y directions, respectively, d is the grid size in both x and y directions. The symbols $(\delta_y \gamma)_{mn}$ and $(\bar{\gamma}^y)_{mn}$ are defined in a similar manner, but with respect to the y direction, and

$$(\bar{\gamma}^{xy})_{mn} \equiv \tfrac{1}{4}(\gamma_{m+1/2,n} + \gamma_{m-1/2,n} + \gamma_{m,n+1/2} + \gamma_{m,n-1/2}). \tag{3.21}$$

4. PHASE TRANSFORMATIONS

In this section we use the Fourier transfer function approach, which is proved to be suitable for use in a comparison of the differential and difference formulations (see [21–23]), to study the semi-discretized schemes (3.9)–(3.13) and (3.14)–(3.18). For the continuous form, the Fourier transform is

$$\hat{A}(k, l, t) = \int_{-\infty}^{+\infty} A(x, y, t) \exp(-i(kx + ly))\, dx\, dy, \tag{4.1}$$

By use of (4.1), Eqs. (3.4)–(3.8) become

$$\frac{\partial \hat{\zeta}}{\partial t} + ik\hat{p} + il\hat{q} = 0, \tag{4.2}$$

$$\frac{\partial \hat{p}}{\partial t} - f\hat{q} + ikgh\hat{\zeta} = 0, \tag{4.3}$$

$$\frac{\partial \hat{q}}{\partial t} + f\hat{p} + ilgh\hat{\zeta} = 0, \tag{4.4}$$

$$\frac{\partial \hat{A}_j}{\partial t} - f\hat{B}_j = 0, \qquad j \geq 1, \tag{4.5}$$

$$\frac{\partial \hat{B}_j}{\partial t} + f\hat{A}_j = 0, \qquad j \geq 1, \tag{4.6}$$

where we have denoted the Fourier transforms by an overlying hat.

The spectral method of order J is the result of solving the first J of Eqs. (4.2)–(4.6) for the $2J+1$ unknowns $\hat{\zeta}, \hat{p}, \hat{q}, \hat{A}_1, \hat{B}_1, \hat{A}_2, \hat{B}_2, \ldots$, after $\hat{A}_{J-1}$ and $\hat{B}_{J-1}$ have been set equal to 0 in the last of these equations. Let $\mathbf{F}$ denote a $(2J+1)$-dimensional column vector defined by

$$\mathbf{F} = [\hat{\zeta}, \hat{p}, \hat{q}, \hat{A}_1, \hat{B}_1, \ldots, \hat{A}_{J-1}, \hat{B}_{J-1}]^{\mathrm{T}}.$$

Then Eqs. (4.2)–(4.6) lead to

$$\frac{\partial \mathbf{F}}{\partial t} + \mathbf{M}\mathbf{F} = 0, \tag{4.7}$$

where $\mathbf{M}$ is a $(2J+1)\times(2J+1)$ matrix given by

$$\mathbf{M} = \begin{pmatrix} 0 & ik & il & 0 & 0 & \cdots & 0 \\ ikgh & 0 & -f & 0 & 0 & \cdots & 0 \\ ilgh & f & 0 & 0 & 0 & \cdots & 0 \\ 0 & 0 & 0 & 0 & -f & \cdots & 0 \\ 0 & 0 & 0 & f & 0 & \ddots & \\ \vdots & \vdots & \vdots & \vdots & \ddots & \ddots & -f \\ 0 & 0 & 0 & 0 & & f & 0 \end{pmatrix}.$$

Similarly, we can obtain from (3.9)–(3.13) that

$$\frac{\partial \mathbf{F}}{\partial t} + \mathbf{M}_B\mathbf{F} = 0, \tag{4.8}$$

where the matrix $\mathbf{M}_B$, which corresponds to the B grid, is of the form

$$\mathbf{M}_B = \begin{pmatrix} 0 & i\alpha & i\beta & 0 & 0 & \cdots & 0 \\ i\alpha gh & 0 & -f & 0 & 0 & \cdots & 0 \\ i\beta gh & f & 0 & 0 & 0 & \cdots & 0 \\ 0 & 0 & 0 & 0 & -f & \cdots & 0 \\ 0 & 0 & 0 & f & 0 & \ddots & \\ \vdots & \vdots & \vdots & \vdots & \ddots & \ddots & -f \\ 0 & 0 & 0 & 0 & & f & 0 \end{pmatrix},$$

where

$$\alpha = \frac{2}{d}\sin\left(\frac{kd}{2}\right)\cos\left(\frac{ld}{2}\right), \qquad \beta = \frac{2}{d}\cos\left(\frac{kd}{2}\right)\sin\left(\frac{ld}{2}\right). \tag{4.9}$$

Moreover, the C grid (recall (3.14)–(3.18)) yields

$$\frac{\partial \mathbf{F}}{\partial t} + \mathbf{M}_C\mathbf{F} = 0, \tag{4.10}$$

with

$$\mathbf{M}_C = \begin{pmatrix} 0 & ia & ib & 0 & 0 & \cdots & 0 \\ iagh & 0 & -fR & 0 & 0 & \cdots & 0 \\ ibgh & fR & 0 & 0 & 0 & \cdots & 0 \\ 0 & 0 & 0 & 0 & -fR & \cdots & 0 \\ 0 & 0 & 0 & fR & 0 & \ddots & \\ \vdots & \vdots & \vdots & \vdots & \ddots & \ddots & -fR \\ 0 & 0 & 0 & 0 & & fR & 0 \end{pmatrix},$$

where

$$a = \frac{2}{d}\sin\left(\frac{kd}{2}\right), \qquad b = \frac{2}{d}\sin\left(\frac{ld}{2}\right), \qquad R = \cos\left(\frac{kd}{2}\right)\cos\left(\frac{ld}{2}\right). \tag{4.11}$$

Further, we seek for the field variable solutions with real wave numbers k, l and complex frequency $\omega(k, l)$. Namely, let

$$\mathbf{F} = \exp(i\omega t)[\hat{\zeta}_0, \hat{p}^0, \hat{q}^0, \hat{A}_1^0, \hat{B}_1^0, \ldots, \hat{A}_{J-1}^0, \hat{B}_{J-1}^0]^{\mathrm{T}}. \tag{4.12}$$

Substituting (4.12) into (4.7), (4.8), and (4.10), and solving the resulting determinants respectively, we obtain the eigenvalues

Differential case,

$$\omega_0 = 0, \tag{4.13}$$

$$\omega_{\pm j} = \pm f, \qquad j = 1, \ldots, J-1, \tag{4.14}$$

$$\omega_{\pm J} = \pm\sqrt{f^2 + gh(k^2+l^2)}; \tag{4.15}$$

B grid

$$\omega_0 = 0, \tag{4.16}$$

$$\omega_{\pm j} = \pm f, \qquad j = 1, ..., J-1, \tag{4.17}$$

$$\omega_{\pm J} = \pm\sqrt{f^2 + gh(\alpha^2 + \beta^2)}; \tag{4.18}$$

C grid,

$$\omega_0 = 0, \tag{4.19}$$

$$\omega_{\pm j} = \pm fR, \qquad j = 1, ..., J-1, \tag{4.20}$$

$$\omega_{\pm J} = \pm\sqrt{(fR)^2 + gh(a^2 + b^2)}. \tag{4.21}$$

The analysis above suggests that if discretized schemes are used then the wave numbers and the Coriolis term will be replaced by some corresponding approximations. These approximations are listed in the following table:

	x-direction	y-direction	Coriolis term
Differential case	k	l	f
B grid	α	β	f
C grid	a	b	Rf

5. NUMERICAL RESULTS

Before presenting the numerical results, we introduce some physical parameters which will be used below. The

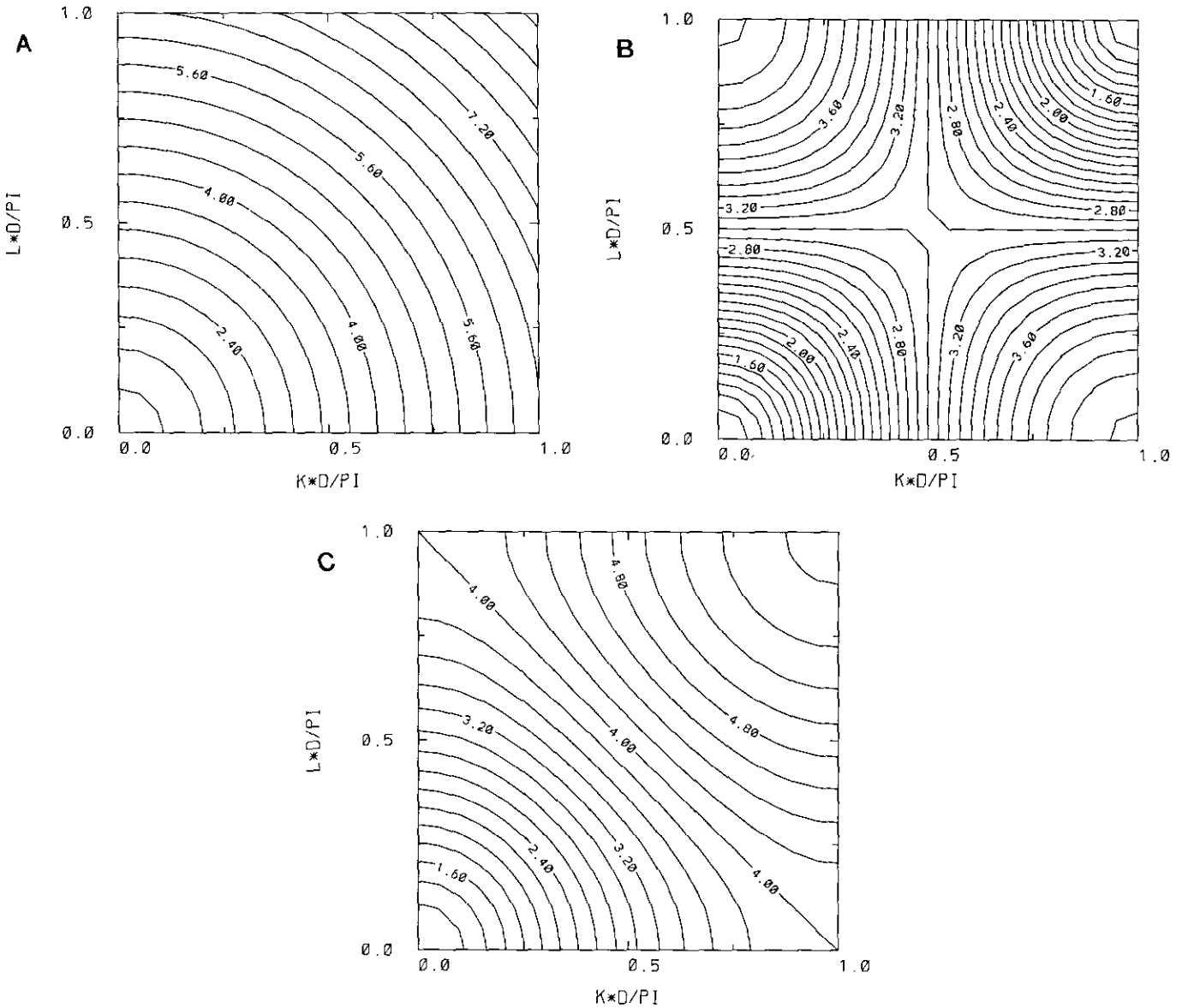

FIG. 2. Contours of the dispersion relations for the differential case, the B and C grids, plotted for $\lambda/d = 2$: (a) 1.6 to 8.8, interval 0.4; (b) 1.1 to 4.1, interval 0.1; (c) 1.2 to 5.6, interval 0.2.

Rossby radius of deformation is basically the horizontal scale at which rotation effects become as important as buoyancy in the rotating fluid of ocean or atmosphere. The Rossby radius of deformation is defined as $\lambda = \sqrt{gh}/f$ with g the acceleration of gravity and h the depth of the fluid. Wave numbers in the x and y directions, k and l, are defined in the region $(k, l) \in (-\pi/d, \pi/d) \times (-\pi/d, \pi/d)$ with d the spatial grid size. The ratio of Rossby radius of deformation λ and the scale length d, $r = \lambda/d$, plays an important role in the present problem. Since the Rossby radius of deformation is fixed, a large ratio corresponds to a small scale length while a small ratio corresponds to a large scale length.

5.1. *Dispersion Analysis*

Dispersion is the interference of Fourier modes that comes about if the waves numbers k and l and the frequency ω are related nonlinearly. In general, the dispersion relation for a partial differential equation is a polynomial of k and l, while a discrete model amounts to a trigonometric approximation. It has been noted that even if the von Neuman condition is satisfied, numerical schemes may be unstable due to the dispersion (see, e.g., [25, 26]). Therefore it is necessary to construct numerical schemes with lower dispersion.

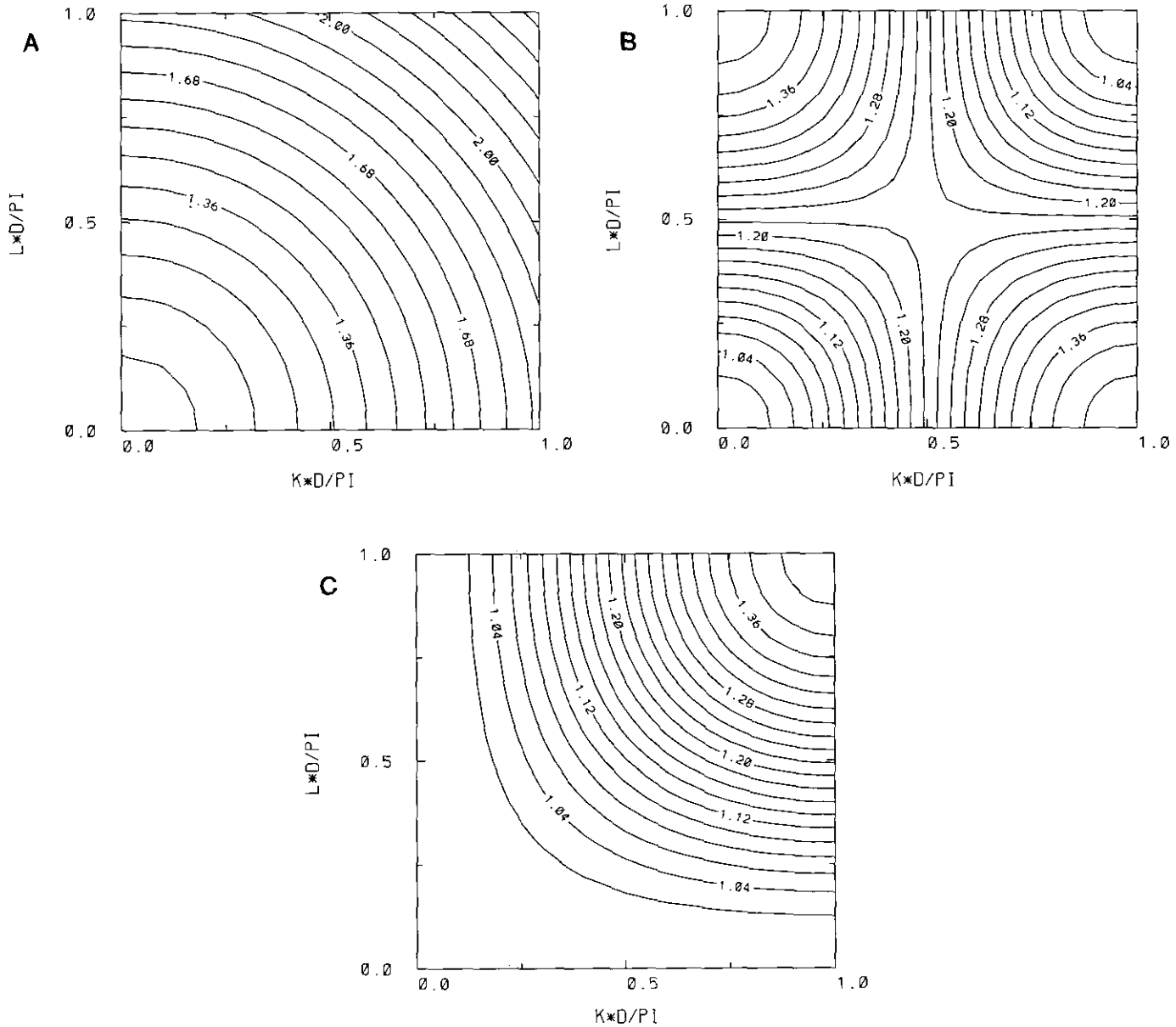

FIG. 3. Contours of the dispersion relations for the differential case, the B and C grids, plotted for $\lambda/d = 0.5$: (a) 1.04 to 2.40, interval 0.08; (b) 1.02 to 1.40, interval 0.02; (c) 1.02 to 1.40, interval 0.02.

In Section 4 the dispersion relations for both B grid and C grid are obtained. It can be seen from (4.13)–(4.15) and (4.16)–(4.18) that the Coriolis term f does not introduce any dispersions when the B grid is employed. However, by comparing (4.13)–(4.15) and (4.19)–(4.21) we can see that the Coriolis term does produce dispersions if the C grid is used. This is due to the fact that in using the C grid the two horizontal velocity components are computed at different spatial points and the Coriolis terms in each momentum equation are averaged over the four neighboring points. This kind of average in the interior points will introduce dispersions. Moreover, when adjacent to a coast, one or more of these four points will in fact lie on the coast and the velocity components at such points are set to zero in most conventional algorithms. The four-point average will result in incorrect values in the interior points, which leads to spurious velocity distributions near the coast [12]. However, if the B grid is used then the two horizontal velocity components are computed at the same spatial points and the Coriolis terms in each momentum equation can be obtained simultaneously. It has been found that the B grid does not produce spurious velocities near the coast [17, 24].

The $\pm J$th eigenvalues in (4.15), (4.18), and (4.21) are the most complicated dispersion relations and a detailed comparison will be given in the following. Figures 2 and 3 show the contours of the dispersion relations for the differential case and the B and C grids plotted for $r = \lambda/d = 2$ and 0.5, respectively. It can be observed from Fig. 2 that in the case of small scale length (i.e., $d < \lambda$) both the B and C grids yield good approximations for the semidiscrete dispersion relations of the differential equations when the wave numbers k and l are small. When k and l are not close to the origin the C grid gives a better approximation to the differential case than the B grid. This suggests that in the case $d < \lambda$ the C grid is more appropriate than the B grid in comparison with the first mode eigenvalues, $\omega_{\pm J}$. Further, it can be seen from Fig. 3 that, if $d > \lambda$, the dispersion relations for the C grid do not lead to reasonable approximations for those of the differential case, except when the wave numbers k and l are very close to the origin. However, the B grid is found still to be appropriate in approximating the dispersive relations of the differential equations for quite large wave numbers.

5.2. *Group Velocity Analysis*

If the dispersion relation takes the form $\omega = \omega(k, l)$, then the group velocity is defined by

$$\mathbf{C} = \left(\frac{\partial \omega}{\partial k}, \frac{\partial \omega}{\partial l}\right). \tag{5.1}$$

This formula is readily established by a stationary phase argument as in [20, 27]. Most nontrivial physical problems in several dimensions will usually be modeled on a regrettably coarse mesh, so group velocity errors will be hardly avoidable. Further, because of the anisotropy of the finite difference grid itself, (5.1) will imply that coarsely represented waves in two-dimensional difference models travel, not only at the wrong speed, but also in the wrong direction (see, e.g., [25]).

It has been observed from (4.13)–(4.15), (4.16)–(4.18), and (4.19)–(4.21) that the last two eigenvalues, $\omega_{\pm J}$, are the dominant terms among all of the eigenpairs. Now let $\omega = \omega_J$

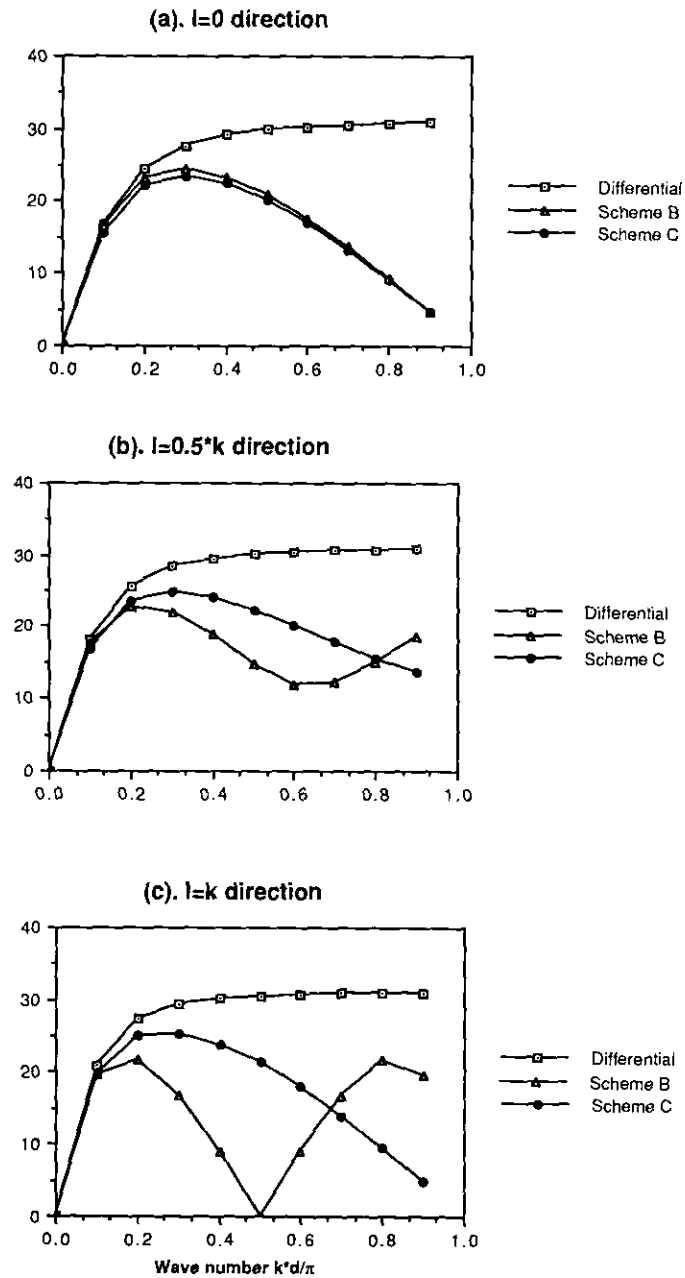

FIG. 4. Group speed relations for the differential case, the B and C grids, plotted for $\lambda/d = 2$ and (a) $l = 0$; (b) $l = 0.5k$; (c) $l = k$.

and we shall consider the group velocities for the differential case, the B and C grids related to this (dominant) eigenvalue (or, dispersion relation). From (4.15), (4.18), and (4.21) we can obtain the governing equations for the group velocity:

Differential case,

$$\frac{\partial \omega_D}{\partial k} = \frac{ghk}{\omega_D}, \qquad \frac{\partial \omega_D}{\partial l} = \frac{ghl}{\omega_D}; \tag{5.2}$$

B grid,

$$\frac{\partial \omega_B}{\partial k} = \frac{gh \sin(kd)\cos(ld)}{\omega_B d}, \qquad \frac{\partial \omega_B}{\partial l} = \frac{gh \sin(ld)\cos(kd)}{\omega_B d}; \tag{5.3}$$

C grid,

$$\frac{\partial \omega_C}{\partial k} = \frac{gh \sin(kd)(1-\varrho^2\cos^2(ld/2))}{\omega_C d}, \qquad \frac{\partial \omega_C}{\partial l} = \frac{gh \sin(ld)(1-\varrho^2\cos^2(kd/2))}{\omega_C d}; \tag{5.4}$$

where $\varrho = d/2\lambda = 1/2r$ and ω_D, ω_B, and ω_C are the frequencies for the differential case, the B grid, and the C grid, respectively. Further, their group speeds (cf. [25]) have the forms

$$|\mathbf{C}_D| = gh\sqrt{k^2+l^2}/\omega_D, \tag{5.5}$$

$$|\mathbf{C}_B| = gh\sqrt{\left(\begin{matrix}\sin^2(kd)\cos^2(ld)\\ +\sin^2(ld)\cos^2(kd)\end{matrix}\right)}\Big/(\omega_B d), \tag{5.6}$$

$$|\mathbf{C}_C| = gh\sqrt{\left(\begin{matrix}\sin^2(kd)[1-\varrho^2\cos^2(ld/2)]^2\\ +\sin^2(ld)[1-\varrho^2\cos^2(kd/2)]^2\end{matrix}\right)}\Big/(\omega_C d). \tag{5.7}$$

The corresponding group propagation angles (from the x-axis) are

$$\theta_D = \tan^{-1}\frac{l}{k}, \tag{5.8}$$

$$\theta_B = \tan^{-1}\frac{\sin(ld)\cos(kd)}{\sin(kd)\cos(ld)}, \tag{5.9}$$

$$\theta_C = \tan^{-1}\frac{\sin(ld)[1-\varrho^2\cos^2(kd/2)]}{\sin(kd)[1-\varrho^2\cos^2(ld/2)]}. \tag{5.10}$$

It can be seen from (5.5)–(5.10) that the velocity speeds and angles are symmetric with respect to k, l and the lines $l = \pm k$. Therefore we shall consider the first half-quarter of (k, l) space only, i.e., $l = \eta k$ with $k \geqslant 0$ and $\eta \in [0, 1]$. To compare the relations of (5.5)–(5.7) we plot the group speeds for some selected directions by setting $\eta = 0$, 0.5, and 1. Figures 4 and 5 show the group speeds in the cases $r = \lambda/d = 2$ and 0.5, respectively. In the case that $r = 2$ it can be observed from Fig. 4 that the two discrete group speeds approximate the continuous one quite accurately when k and l are small. Similar to our observations for the dispersion relation, the C grid is more appropriate than the B grid when k and l are larger. In the case that $r = 0.5$, it is observed from Fig. 5a that the group speed of the C grid does not

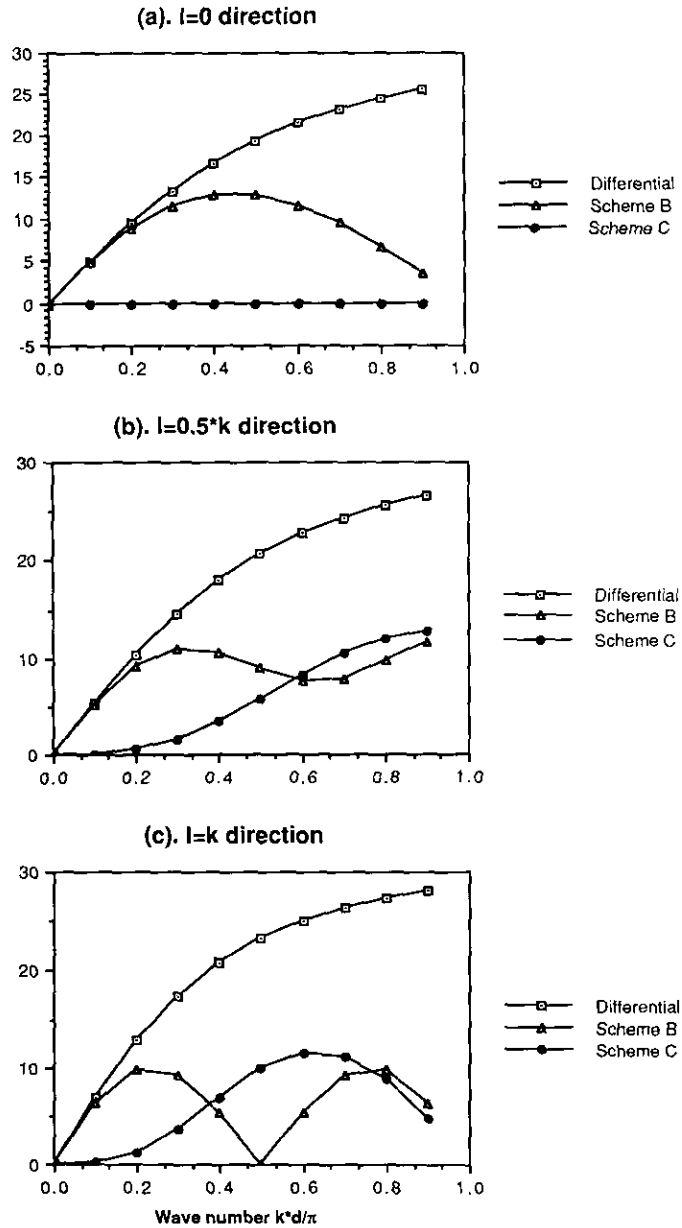

FIG. 5. Group speed relations for the differential case, the B and C grids, plotted for $\lambda/d = 0.5$ and (a) $l = 0$; (b) $l = 0.5k$; (c) $l = k$.

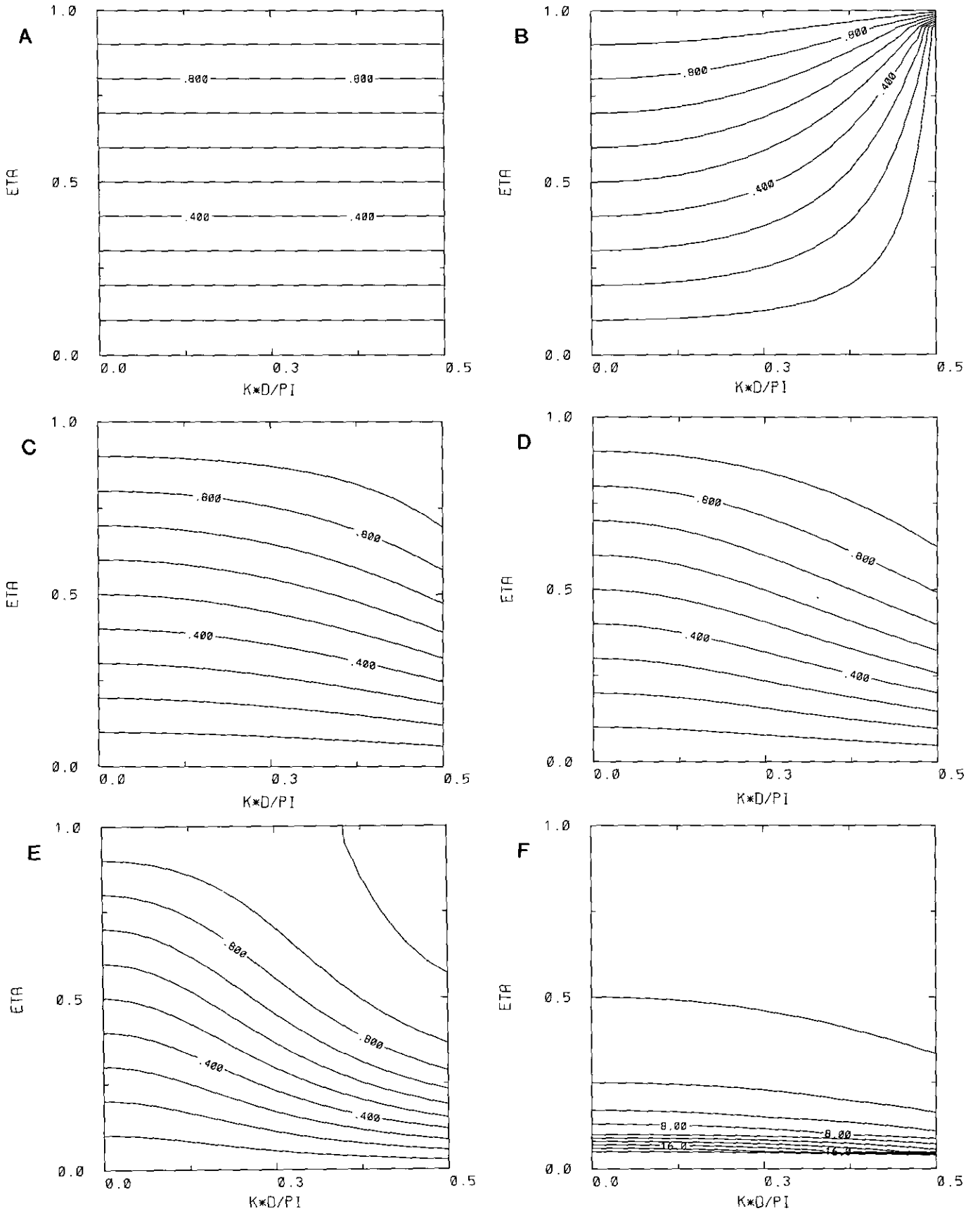

FIG. 6. Contours of the tangents of the group propagation angle, plotted for (a) the differential case; (b) the B grid; (c) the C grid with $r = 2$; (d) the C grid with $r = 1$; (e) the C grid with $r = \frac{2}{3}$, and (f) the C grid with $r = 0.5$.

approximate the continuous solution even when $l=0$ and k is very small. Further, it can be obtained from (5.8)–(5.10) that if $l \equiv 0$ then $\theta_D = \theta_B = \theta_C$. However, if $l \not\equiv 0$, then the discrete group velocities do not travel in the exactly same direction of the continuous one. To see this we consider the case $l = \eta k$ with $0 < \eta < 1$. Figure 6 shows the contours of the tangents of the angles with $\eta \in (0, 1)$ for the differential solution (Fig. 6a) and the B grid solution (Fig. 6b). Also shown are the C grid results for $r = 2$, 1, $\frac{2}{3}$, and 0.5 (Figs. 6c–f). Figure 6 suggests that the reliability of the C grid decreases as r decreases. If $r > 1$ (i.e., $d < \lambda$) then the C grid gives more accurate approximation to θ_D than the B grid does. However, in the case $r < 1$ more accurate results are obtained by using the B grid. In practice, it is important that numerical schemes should approximate the continuous solutions of small wave numbers. However, Fig. 5 and 6 imply that when $r = 0.5$ the C grid is not appropriate for small values of wave number and is unlikely to produce accurate numerical solutions in the practical calculations.

6. CONCLUSION

In this work we have investigated the B and C grids by comparing their dispersion and group velocity relations. In the conclusion we give a summary of the points we have raised in the present work. Once again: d is the spatial grid size, λ is the Rossby radius of deformation, k and l are wave numbers in the x and y directions, respectively.

- Coriolis term f introduces dispersions for the C grid but not for the B grid.
- If the horizontal scale length is less than the Rossby radius of deformation, i.e., $d < \lambda$, then the C grid is more appropriate than the B grid. The B grid is accurate only when the wave numbers k and l are small.
- If the horizontal scale length is greater than the Rossby radius of deformation, i.e., $d > \lambda$, then the B grid is more appropriate than the C grid. The C grid gives unreasonable group velocity even when the wave numbers are very small.

It should be pointed out that Eqs. (3.4)–(3.6) are equivalent to the linearized shallow-water equations. Since it is (3.4)–(3.6) which yield the eigenvalues $\omega_{\pm J}$ (the frequencies of the inertia–gravity modes for the shallow water equations), the analysis and the results in Section 5 are directly applicable to the shallow-water equations.

ACKNOWLEDGMENTS

The authors thank Professor I. M. Navon for bringing this problem to their attention. We are also grateful to Professor R. W. Lardner and the referees for many helpful comments and suggestions which have improved the presentation and content of this paper. This research was supported by the Natural Sciences and Engineering Research Council of Canada (NSERC Operating Grant OGP0105545).

REFERENCES

1. A. Arakawa and V. R. Lamb, in *Methods in Computational Physics*, Vol. 17 (Academic Press, New York, 1977), p. 174.
2. A. Arakawa and V. R. Lamb, *Mon. Weather Rev.* **109**, 18 (1981).
3. J. O. Backhaus, *Dtsch. Hydrogr. Z.* **38**, 165 (1985).
4. A. M. Davis, *Appl. Math. Model.* **4**, 245 (1980).
5. A. M. Davis, *Int. J. Num. Methods Fluids* **3**, 33 (1983).
6. R. T. Gedney and W. Lick, *J. Geophys. Res.* **77**, 2714 (1972).
7. D. B. Haidvogel, J. L. Wilkin, and R. E. Young, *J. Comput. Phys.* **94**, 151 (1991).
8. G. J. Haltiner and R. T. Williams, *Numerical Prediction and Dynamic Meteorology* (Wiley, New York, 1980).
9. W. Hansen, in *Proceedings, Symp. Hydrodyn. Phys. Oceanog., Institut für Meereskunde, Universität Hamburg*, 1962, p. 24.
10. N. S. Heaps, *Mem. Soc. R. Sci. Liege* **6**, 143 (1972).
11. N. S. Heaps, *Geophys. J. Roy. Astron. Soc.* **64**, 290 (1981).
12. B. M. Jamart and J. Ozer, *J. Geophys. Res.* **91**, 10621 (1986).
13. B. Johns, P. C. Sinha, S. K. Dube, U. C. Mohanty, and A. D. Rao, *Q. J. R. Meteorol. Soc.* **109**, 211 (1983).
14. R. W. Lardner, *J. Geophys. Res.* **95**, 22269 (1990).
15. R. W. Lardner and H. M. Cekirge, *Appl. Math. Model.* **12**, 471 (1988).
16. R. W. Lardner and P. Smoczynski, *Proc. R. Soc. London A* **430**, 263 (1990).
17. R. W. Lardner and Y. Song, *Int. J. Num. Methods Fluids* **14**, 109 (1992).
18. R. W. Lardner and Y. Song, *J. Comput. Phys.*, in press.
19. J. J. Leendertse, *Rand Corp. Tech. Rep.* RM-5294-PR, 1967.
20. J. Lighthill, *Waves in Fluids* (Cambridge University Press, 1978).
21. B. Neta and I. M. Navon, *J. Comput. Phys.* **81**, 277 (1989).
22. A. L. Schoenstadt, *J. Comput. Phys.* **23**, 364 (1977).
23. A. L. Schoenstadt, *Mon. Weather Rev.* **108**, 12488 (1980).
24. Y. Song, Ph. D. thesis, Simon Fraser University, BC, Canada, 1990 (unpublished).
25. L. N. Trefethen, *SIAM Rev.* **24**, 113 (1982).
26. L. N. Trefethen, in *Numerical Analysis 1986*, edited by D. F. Griffiths and G. A. Watson (Longman, 1986), p. 200.
27. G. Whitham, *Linear and Nonlinear Waves* (Wiley-Interscience, New York, 1974).
28. R. T. Williams, *Mon. Weather Rev.* **109**, 463 (1981).
29. F. J. Winninghoff, Ph. D. thesis, Department of Meteorology, University of California, Los Angeles, 1968 (unpublished).